Computer Assisted Mechanics and Engineering Sciences, 10: 575–585, 2003.


# Analytical formulation of hybrid–Trefftz thick plate elements

J. Petrolito
*La Trobe University, Bendigo, Australia*

(Received September 11, 2003)

This paper discusses a domain-based formulation for hybrid–Trefftz thick plate elements. The formulation can be applied to triangular and quadrilateral elements, and enables an analytical formulation of these elements to be used. Techniques for improving the computational efficiency are explored, and a simple and accurate triangular element is formulated in this manner.

## 1. Introduction

The analysis of plate structures is of fundamental importance in structural engineering. While the theoretical formulation of the problem is straightforward, the resulting partial differential equations are difficult to solve analytically except for simple structures. Hence, a finite element solution is required for most practical problems, and numerous elements have been developed for the plate bending problem [1].

The early elements were based on classical, thin plate theory [2]. In this case, a conforming element requires $C_1$ continuity, which is difficulty to achieve. The $C_1$ continuity requirement can be avoided by using Mindlin's shear deformation theory [3]. This theory uses independent assumptions for the transverse displacement and normal rotations, and $C_0$ approximations can be used. Unfortunately, this approach is not completely foolproof, and it can also have problems. The two major problems are the possibility of spurious mechanisms and locking for thin plates.

The locking problem can be avoided by using consistent internal approximations [4–6]. The key requirement for the approximations is that they must satisfy the governing differential equations. This requirement also naturally suggests the hybrid–Trefftz formulation [7] as a basis for deriving thick plate elements.

The required solutions for Mindlin's theory are given in [5, 8]. The solutions given in [5] are polynomial-based, but are incomplete in the Trefftz sense. In contrast, the solutions given in [8] include Bessel functions, and are complete. The polynomial solutions are suitable for deriving low-order elements for use in an h-adaptive strategy or an hp-adaptive strategy. However, they are not suitable for use in a purely p-adaptive strategy.

The hybrid–Trefftz formulation is based on independent approximations for the internal and boundary displacements of the element. In the standard approach, the derivation of the element properties is based on integrals, usually performed numerically, around the boundary of the element. The advantage of this approach is that element shape functions only need to be defined on the boundary, and this allows elements with an arbitrary polygonal shape to be derived. A numerical inversion of the element flexibility matrix, $\mathbf{H}$, is required to evaluate the element stiffness matrix, $\mathbf{K}$.

The numerical integration and inversion are computationally expensive. Hence, the efficiency of hybrid–Trefftz elements can be significantly improved if either or both of these requirements are eliminated. Numerical integration can be avoided by introducing shape functions that are defined throughout the element, and reformulating the method using domain integrals. This approach is

simplest for triangular and quadrilateral elements, and hence restricts the geometry of the resulting elements. However, this restriction is not severe since triangular and quadrilateral elements can be used to analyse regions of arbitrary geometry.

The evaluation of $\mathbf{K}$ can be significantly improved if $\mathbf{H}$ is simple to invert, and ideally $\mathbf{H}$ should be a diagonal matrix [9]. To achieve this for thick plate elements, the original polynomial functions from [5] are combined to produce new functions that are energy-orthogonal. The resulting functions depend on the geometric properties of the element.

These two modifications result in a highly efficient implementation, and in principle the technique can be used for any element. However, the energy-orthogonal functions become more complicated as the order of the elements increases. Hence, the paper also discusses the practical limitations of this approach.

## 2. Governing equations

Mindlin's theory [3] is based on independent approximations for the transverse displacement, $w$, and the rotations $\theta_x$ and $\theta_y$ (see Fig. 1). In contrast to thin plate theory, both bending and transverse shear strains are present. These are given by

$$\boldsymbol{\epsilon}_b = \begin{bmatrix} \partial/\partial x & 0 \\ 0 & \partial/\partial y \\ \partial/\partial y & \partial/\partial x \end{bmatrix} \begin{Bmatrix} \theta_x \\ \theta_y \end{Bmatrix} = \mathbf{L}_1 \boldsymbol{\theta}, \tag{1a}$$

$$\boldsymbol{\epsilon}_s = \begin{Bmatrix} \partial/\partial x \\ \partial/\partial y \end{Bmatrix} w - \boldsymbol{\theta} = \mathbf{L}_2 w - \boldsymbol{\theta}, \tag{1b}$$

where $\boldsymbol{\epsilon}_b$ is the bending strain vector and $\boldsymbol{\epsilon}_s$ is the shear strain vector, which is zero in the thin plate limit.

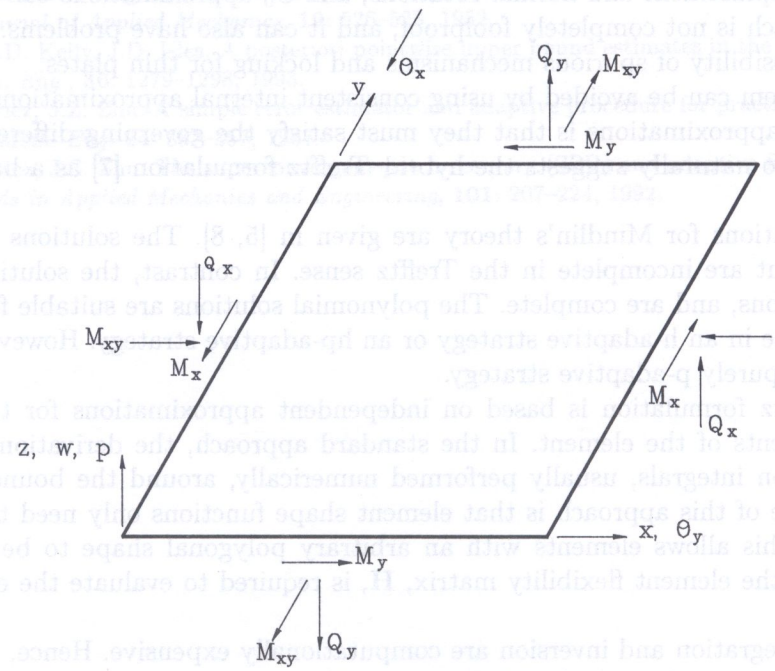


**Fig. 1.** Sign convention

For an isotropic material, bending moments and shear forces are given in terms of the strains by

$$\mathbf{M} = \begin{Bmatrix} M_x \\ M_y \\ M_{xy} \end{Bmatrix} = -D \begin{bmatrix} 1 & \nu & 0 \\ \nu & 1 & 0 \\ 0 & 0 & (1-\nu)/2 \end{bmatrix} \boldsymbol{\epsilon}_b = -\mathbf{D}\boldsymbol{\epsilon}_b, \tag{2a}$$

$$\mathbf{Q} = \begin{Bmatrix} Q_x \\ Q_y \end{Bmatrix} = kGh\boldsymbol{\epsilon}_s. \tag{2b}$$

In Eq. (2), $D = Eh^3/[12(1-\nu^2)]$ is the bending rigidity, $E$ is Young's modulus, $\nu$ is Poisson's ratio, $G = E/[2(1+\nu)]$ is the shear modulus, $h$ is the plate thickness and $k$ is a correction factor, which is usually taken as $5/6$ or $\pi^2/12$.

The static equilibrium equations for Mindlin's theory are

$$\mathbf{Q} + \mathbf{L}_1^T\mathbf{M} = \mathbf{0}, \tag{3a}$$

$$\mathbf{L}_2^T\mathbf{Q} + p = 0, \tag{3b}$$

where $p$ is the applied transverse load on the plate.

Combining Eq. (1)–(3) gives the governing equations, namely

$$kGh(\mathbf{L}_2 w - \boldsymbol{\theta}) + \mathbf{L}_1^T\mathbf{D}\mathbf{L}_1\boldsymbol{\theta} = \mathbf{0}, \tag{4a}$$

$$kGh\mathbf{L}_2^T(\mathbf{L}_2 w - \boldsymbol{\theta}) + p = 0. \tag{4b}$$

Equation (4) represents a system of three coupled equations of order six, and requires the specification of three boundary conditions on any portion of the plate boundary.

## 3. Element approximations

In the current formulation, two independent approximations are used for the element that are linked via a hybrid–Trefftz variational principle to produce the element equations.

### 3.1. Internal approximations

In the interior of each element, the assumed displacement and rotations are chosen so that the locking problem is eliminated a priori. This is done by using approximations that automatically satisfy the static and homogeneous version of governing differential equations (Eq. (4)).

Firstly, the element rotations are taken as

$$\boldsymbol{\theta} = \mathbf{L}_2 w + R\mathbf{L}_3 w, \tag{5}$$

where

$$\mathbf{L}_3 = \begin{bmatrix} \partial^3/\partial x^3 + \partial^3/\partial x \partial y^2 \\ \partial^3/\partial y^3 + \partial^3/\partial x^2 \partial y \end{bmatrix}, \tag{6}$$

and

$$R = \frac{D}{kGh} = \frac{h^2}{6k(1-\nu)}, \tag{7}$$

is the ratio of the flexural rigidity to the shear rigidity.

Hence, the rotations are given by the thin plate expression, $\boldsymbol{\theta} = \mathbf{L}_2 w$, plus a correction term that is a function of the thickness of the plate. In the thin plate limit ($R = h = 0$), Eq. (5) is consistent with the constraint $\boldsymbol{\theta} = \mathbf{L}_2 w$, and locking will not occur.

Secondly, the transverse displacement is approximated by biharmonic polynomials, which are generated using [7]

$$w_{j+1} = r^2 \operatorname{Re} z^m, \tag{8a}$$

$$w_{j+2} = r^2 \operatorname{Im} z^m, \tag{8b}$$

$$w_{j+3} = \operatorname{Re} z^{m+2}, \tag{8c}$$

$$w_{j+4} = \operatorname{Im} z^{m+2}, \tag{8d}$$

for $m = 0, 1, 2, \ldots$, where $z = x + iy$, $r^2 = x^2 + y^2$ and Re and Im denote the real and imaginary parts of a complex number.

Hence, the internal element approximations are given by

$$\mathbf{u} = \mathbf{P}\boldsymbol{\beta} + \mathbf{u}_o, \tag{9a}$$

$$\boldsymbol{\epsilon} = \mathbf{L}\mathbf{u} = \mathbf{B}_\beta \boldsymbol{\beta} + \boldsymbol{\epsilon}_o, \tag{9b}$$

$$\boldsymbol{\sigma} = \mathbf{E}\boldsymbol{\epsilon} = \mathbf{S}_\beta \boldsymbol{\beta} + \boldsymbol{\sigma}_o, \tag{9c}$$

where

$$\mathbf{u} = \begin{Bmatrix} w \\ \theta \end{Bmatrix}, \quad \boldsymbol{\epsilon} = \begin{Bmatrix} \boldsymbol{\epsilon}_b \\ \boldsymbol{\epsilon}_s \end{Bmatrix}, \quad \boldsymbol{\sigma} = \begin{Bmatrix} \mathbf{M} \\ \mathbf{Q} \end{Bmatrix}. \tag{10}$$

In Eq. (9), $\mathbf{P}$ contains $M$ solutions generated from Eqs. (5) and (8), $\mathbf{u}_o$ is a particular solution for the given loading and $\boldsymbol{\beta}$ is a vector of unknown parameters. The $\boldsymbol{\beta}$ parameters are local to each element, and are eliminated at the element level.

The shear forces are independent of the shear rigidity, and hence no numerical difficulties occur in calculating shear forces for all values of the plate thickness. In contrast, numerical difficulties can occur in conventional displacement formulations using Eq. (2) for thin plates [10].

### 3.2. Boundary approximations

To ensure that displacements and rotations are continuous between adjacent elements, independent boundary approximations are introduced by

$$\tilde{\mathbf{u}} = \mathbf{N}_b \mathbf{q}, \tag{11}$$

where

$$\tilde{\mathbf{u}} = \begin{Bmatrix} \tilde{w} \\ \tilde{\theta} \end{Bmatrix}, \tag{12}$$

$\mathbf{q}$ is the element degrees of freedom vector and $\mathbf{N}_b$ is the boundary shape function vector, which is continuous around the boundary of the element. The collection of the element $\mathbf{q}$ vectors gives the global variables for the plate system being analysed.

## 4. Element matrices

The element matrices are derived from the element approximations as discussed below.

### 4.1. Boundary formulation

The formulation is based on the hybrid-Trefftz variational principle, which was originally developed for thin plate problems by Jirousek [7]. For the current problem, the appropriate functional is [5]

$$\Pi_H = \frac{1}{2}\int_S \boldsymbol{\sigma}^T \mathbf{T}_\sigma^T \mathbf{u}\,\mathrm{d}S - \int_S \boldsymbol{\sigma}^T \mathbf{T}_\sigma^T \tilde{\mathbf{u}}\,\mathrm{d}S + \int_{S_2} \overline{\boldsymbol{\sigma}}^T \mathbf{T}_\sigma^T \tilde{\mathbf{u}}\,\mathrm{d}S, \tag{13}$$

where $\mathbf{T}_\sigma$ is a transformation matrix, $\overline{\boldsymbol{\sigma}}$ contains the prescribed boundary moments and shear forces, $S$ is the total boundary of the element and $S_2$ is the boundary of the element where moments and shear forces are specified.

Substituting the element approximations from Eqs. (9) and (11) into equation (13) gives

$$\Pi_H = \frac{1}{2}\boldsymbol{\beta}^T \mathbf{H}\boldsymbol{\beta} + \boldsymbol{\beta}^T \mathbf{H}_o - \boldsymbol{\beta}^T \mathbf{G}\mathbf{q} + \mathbf{q}^T \mathbf{R}_q, \tag{14}$$

where the matrices in Eq. (14) are all evaluated in terms of boundary integrals [5]. However, the details are omitted since they are not required in this paper.

Since the variables $\boldsymbol{\beta}$ are only defined locally within each element, they can be eliminated at the element level. Setting the first variation of $\Pi_H$ with respect to $\boldsymbol{\beta}$ to zero and solving gives

$$\boldsymbol{\beta} = \mathbf{H}^{-1}(\mathbf{G}\mathbf{q} - \mathbf{H}_o). \tag{15}$$

Hence,

$$\Pi_H = -\frac{1}{2}\mathbf{q}^T \mathbf{K}\mathbf{q} + \mathbf{q}^T \mathbf{R}, \tag{16}$$

where

$$\mathbf{K} = \mathbf{G}^T \mathbf{H}^{-1} \mathbf{G}, \tag{17a}$$

$$\mathbf{R} = \mathbf{R}_q + \mathbf{G}^T \mathbf{H}^{-1} \mathbf{H}_o. \tag{17b}$$

The above formulation allows elements of arbitrary polygonal shape to be derived, and is thus a very flexible formulation. However, the matrices in Eq. (14) need to be numerically integrated, and there is a significant cost associated with the inversion of $\mathbf{H}$ in Eq. (15). Hence, an alternative formulation is adopted below to avoid these computational costs, and make the elements more efficient.

### 4.2. Domain formulation

To use alternate domain integrals in $\Pi_H$, internal approximations consistent with the boundary displacements from Eq. (11) are introduced as

$$\tilde{\mathbf{u}} = \mathbf{N}\mathbf{q}, \tag{18a}$$

$$\tilde{\boldsymbol{\epsilon}} = \mathbf{L}\tilde{\mathbf{u}} = \mathbf{B}\mathbf{q}, \tag{18b}$$

$$\tilde{\boldsymbol{\sigma}} = \mathbf{E}\tilde{\boldsymbol{\epsilon}} = \mathbf{S}\mathbf{q}, \tag{18c}$$

where the shape function matrix $\mathbf{N}$ is consistent with the boundary shape function matrix in Eq. (11). Hence, in terms of domain integrals the equivalent functional is

$$\Pi_H = \frac{1}{2}\int_A \boldsymbol{\epsilon}^T \mathbf{E}\boldsymbol{\epsilon}\,\mathrm{d}A - \int_A \boldsymbol{\epsilon}^T \mathbf{E}\tilde{\boldsymbol{\epsilon}}\,\mathrm{d}A + \int_A \tilde{\mathbf{u}}^T \mathbf{p}\,\mathrm{d}A + \int_{S_2} \overline{\boldsymbol{\sigma}}^T \mathbf{T}_\sigma^T \tilde{\mathbf{u}}\,\mathrm{d}S, \tag{19}$$

where

$$\mathbf{p} = \begin{Bmatrix} p \\ 0 \\ 0 \end{Bmatrix}, \tag{20}$$

and $A$ is the area of the element.

Substituting Eqs. (9) and (11) into Eq. (19) gives the equivalent forms for the element matrices, namely

$$\mathbf{H} = \int_A \mathbf{B}_\beta^T \mathbf{E} \mathbf{B}_\beta \, \mathrm{d}A, \tag{21a}$$

$$\mathbf{H}_o = \int_A \mathbf{B}_\beta^T \mathbf{E} \mathbf{B}_o \, \mathrm{d}A, \tag{21b}$$

$$\mathbf{G} = \int_A \mathbf{B}_\beta^T \mathbf{E} \mathbf{B} \, \mathrm{d}A, \tag{21c}$$

$$\mathbf{G}_o = \int_A \mathbf{B}^T \mathbf{E} \mathbf{B}_o \, \mathrm{d}A, \tag{21d}$$

$$\mathbf{R}_p = \int_A \mathbf{N}^T \mathbf{p} \, \mathrm{d}A, \tag{21e}$$

$$\mathbf{R}_\sigma = \int_{S_2} \mathbf{N}^T \mathbf{T}_\sigma \overline{\boldsymbol{\sigma}} \, \mathrm{d}S, \tag{21f}$$

$$\mathbf{R} = \mathbf{R}_p + \mathbf{R}_\sigma - \mathbf{G}_o + \mathbf{G}^T \mathbf{H}^{-1} \mathbf{H}_o. \tag{21g}$$

The load vectors $\mathbf{R}_p$ and $\mathbf{R}_\sigma$ are the terms that normally arises from a displacement-based finite element formulation. Noting this, a simplifying option is to use

$$\mathbf{R} = \mathbf{R}_p + \mathbf{R}_\sigma, \tag{22}$$

rather than the consistent load vector from Eq. (21).

## 5. Computational aspects

The domain formulation is used to evaluate the element matrices and improve the computational performance of the elements. The critical matrices are $\mathbf{H}$ and $\mathbf{G}$, and hence we concentrate on these below.

### 5.1. Evaluation of H

As mentioned previously, a major computational cost of hybrid–Trefftz elements is the inversion of $\mathbf{H}$. Of course, in practice $\mathbf{H}$ would not be inverted, but rather an equation solver is used to evaluate matrix products of $\mathbf{H}^{-1}$ with other matrices. However, it is convenient to talk of "inverting" $\mathbf{H}$ in the discussion below.

From Eq. (21), matrix $\mathbf{H}$ is obtained from the strain energy of the element. Thus, a typical term, $H_{ij}$, of $\mathbf{H}$ is given by

$$H_{ij} = H_{ji} = \int_A \mathbf{B}_{\beta i}^T \mathbf{E} \mathbf{B}_{\beta j} \, \mathrm{d}A = S[\mathbf{P}_i, \mathbf{P}_j] = S[\mathbf{P}_j, \mathbf{P}_i], \tag{23}$$

where $\mathbf{B}_{\beta i}$ represents the $i$th column of $\mathbf{B}_\beta$, and the notation $S[\mathbf{P}_i, \mathbf{P}_j]$ indicates that the term $H_{ij}$ is a function of $\mathbf{P}_i$ and $\mathbf{P}_j$. In general, $\mathbf{H}$ is a full and symmetric matrix.

For maximum computational efficiency, $\mathbf{H}$ should be a diagonal matrix. The internal approximation functions all satisfy the homogeneous form of the governing differential equations. Hence, linear combinations of these functions are also acceptable approximation functions. This observation can be used to generate modified approximation functions that lead to a diagonal $\mathbf{H}$.

Accordingly, the original functions, $\mathbf{P}$, from Eq. (9) are combined to produce energy-orthogonal functions, $\overline{\mathbf{P}}$, using the Gram-Schmidt method, giving

$$\overline{\mathbf{P}}_1 = \mathbf{P}_1; \quad \overline{\mathbf{P}}_i = \mathbf{P}_i - \sum_{j=1}^{i-1} \frac{S[\mathbf{P}_i, \overline{\mathbf{P}}_j]}{S[\overline{\mathbf{P}}_j, \overline{\mathbf{P}}_j]} \overline{\mathbf{P}}_j, \quad i = 2, 3, \ldots M, \tag{24}$$

where $\mathbf{P}_i$ represents the $i$th column of $\mathbf{P}$.

In principle, Eq. (24) can be used to generate as many energy-orthogonal functions as required. The integrals in Eq. (23) need to be evaluated analytically, and this can be done for triangular and quadrilateral elements using standard integration formulas [1]. The calculations are best carried out using a symbolic manipulation program, such as Reduce or Maple, because of the amount of algebra involved.

In practice, the expressions become excessively complicated with increasing polynomial orders. For the current problem, this occurs for terms higher than cubic order. Hence, for elements that require these higher-order terms, it is preferable to combine energy-orthogonal approximations up to cubic order and standard approximations for higher-order terms, giving a partially-diagonal $\mathbf{H}$. In this case, the inversion of $\mathbf{H}$ can be carried out using block submatrices to take advantage of its partially-diagonal form.

### 5.2. Evaluation of G

Matrix $\mathbf{G}$ is found from the energy coupling between $\mathbf{u}$ and $\widetilde{\mathbf{u}}$, and in general is a full and rectangular matrix. Two alternatives can be used for $\widetilde{\mathbf{u}}$, namely independent approximations and linked approximations [6, 8]. Linked approximations generally improve accuracy, and require fewer internal approximations. For computational efficiency, $\mathbf{G}$ should also be evaluated analytically.

## 6. Matrices for element $\widetilde{\text{T}}$21-7

The above formulation is applicable to any of the elements presented in [5, 6]. In this section, we discuss the procedure for element $\widetilde{\text{T}}$21-7 [6]. This element uses linked quadratic approximations for the boundary displacement and linear approximations for the boundary rotations. These are combined with internal approximations that use seven solutions in Eq. (9). The final degrees of freedom are the displacement and rotations at the corner nodes (see Fig. 2). The element has one benign zero-energy mode, and is thus a robust element for practical problems.

Equation (24) is used to replace the original approximations with energy-orthogonal approximations. The modified transverse displacement terms are

$$\overline{\mathbf{P}}_w = \lfloor x^2 + y^2,\ x^2 - y^2,\ 2xy,\ x^3,\ y^3, \frac{y[I_x(3x^2 - \nu y^2) + AR(3x^2 - y^2)]}{3I_x + AR}, \frac{x[I_y(3y^2 - \nu x^2) + AR(3y^2 - x^2)]}{3I_y + AR}, \tag{25}$$

where

$$I_x = \int_A y^2 \, \mathrm{d}A, \qquad I_y = \int_A x^2 \, \mathrm{d}A. \tag{26}$$

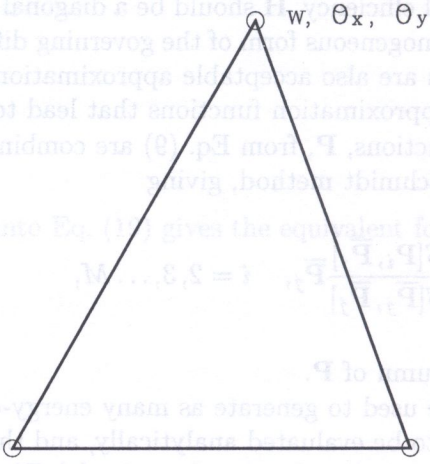


**Fig. 2.** Element $\tilde{\text{T}}$21-7

The coordinates $x$ and $y$ are relative to the centroid of the element, and in the directions of the principal axes. The modified rotation terms are obtained from Eq. (5).

The resulting diagonal $\mathbf{H}$ is given by

$$\mathbf{H} = D\,\text{Diag}\Bigg[8A(1+\nu),\ 8A(1-\nu),\ 8A(1-\nu),\ 36(I_y+AR),\ 36(I_x+AR),$$

$$\frac{4(1-\nu)[2(I_y+AR)I_x+(1+\nu)I_x^2+2I_yAR]}{I_x+AR},$$

$$\frac{4(1-\nu)[2(I_x+AR)I_y+(1+\nu)I_y^2+2I_xAR]}{I_y+AR}\Bigg]. \tag{27}$$

Note that Eqs. (25) and (27) are also applicable to quadrilateral elements.

Matrix $\mathbf{G}$ is evaluated according to Eq. (21), and given in Appendix 1. These expressions are not applicable to quadrilateral elements. As can be seen, the analytical expressions for $\mathbf{H}$ and $\mathbf{G}$ are simple and concise, and both matrices can be evaluated rapidly.

In summary, the proposed procedure improves the computational performance of the elements by (a) deriving analytical expressions for the element matrices and avoiding numerical integrations around the element boundary and (b) avoiding the computational expense of a numerical inversion of $\mathbf{H}$, since this is not required when $\mathbf{H}$ is a diagonal matrix.

## 7. Examples

The goal of the current paper is to improve the computational efficiency of hybrid–Trefftz thick plate elements, rather than to derive new elements. Hence, the numerical results presented previously for element $\tilde{\text{T}}$21-7 [6] remain unchanged. However, the current domain-based formulation has suggested that the simplified load vector from Eq. (22) can be used instead of the consistent load vector from Eq. (21). Hence, two examples are considered in this section to evaluate the effect of this simplification.

In both examples, Poisson's ratio is taken as 0.3 and a shear correction factor of 5/6 is used. The boundary conditions are described as follows:

1. Clamped Support (C): $w = \theta_t = \theta_n = 0$,
2. Hard Simple Support (SS2): $w = \theta_t = M_n = 0$,

where $n$ and $t$ are the normal and tangential axes, respectively, at the boundary.

### 7.1. Uniformly loaded simply supported (SS2) square plate

As a first problem, a square simply supported (SS2) plate of size $a \times a$ and thickness $h$ subjected to a uniform load $p$ is considered. Taking symmetry into account, a quarter of the plate was analyzed using a uniform mesh of $N \times N$ elements (see Fig. 3). Results for the central displacement and bending moment for a thick plate ($a/h = 10$) and a thin plate ($a/h = 100$) are given in Table 1. Subscripts $c$ and $s$ are used to denote the results associated with the consistent and simplified load vectors, respectively. It can be seen that there are only small differences in the results using the alternate load vectors.

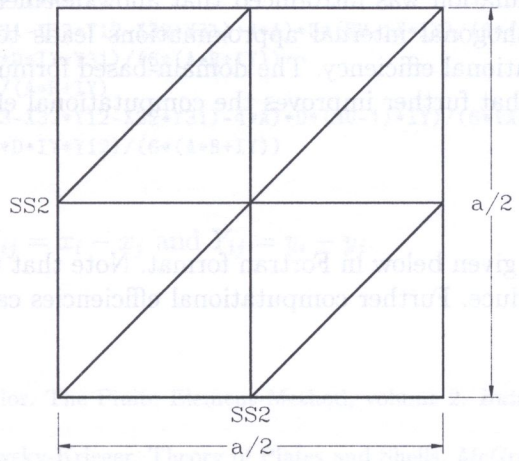


**Fig. 3.** Geometry and mesh for simply supported plate (quarter plate and $N = 2$)

**Table 1.** Central displacement and bending moment for simply supported (SS2) plate subjected to uniform load (displacement multiplier = $10^{-3}pa^4/D$, moment multiplier = $10^{-2}pa^2$)

| | $a/h = 10$ | | | | $a/h = 100$ | | | |
|---|---|---|---|---|---|---|---|---|
| $N$ | $w_c$ | $w_s$ | $M_c$ | $M_s$ | $w_c$ | $w_s$ | $M_c$ | $M_s$ |
| 2 | 4.015 | 4.017 | 4.508 | 4.523 | 3.778 | 3.780 | 4.464 | 4.503 |
| 4 | 4.215 | 4.214 | 4.732 | 4.733 | 3.998 | 3.998 | 4.675 | 4.685 |
| 8 | 4.259 | 4.259 | 4.775 | 4.775 | 4.049 | 4.049 | 4.758 | 4.760 |
| 16 | 4.269 | 4.270 | 4.785 | 4.785 | 4.061 | 4.061 | 4.782 | 4.781 |
| Exact | 4.273 | | 4.789 | | 4.062 | | 4.789 | |

### 7.2. Uniformly loaded clamped square plate

As a second example, the plate was re-analysed using clamped supports, and the results are given in Table 2. The reference values are taken from [8] and [2] for the thick and thin plate cases, respectively. There is virtually no difference in the results using the alternate load vectors. Hence, the simplified load vector can be used to further improve the efficiency of the element without sacrificing accuracy.

**Table 2.** Central displacement and bending moment for clamped plate subjected to uniform load (displacement multiplier = $10^{-3}pa^4/D$, moment multiplier = $10^{-2}pa^2$)

| | $a/h = 10$ | | | | $a/h = 100$ | | | |
|---|---|---|---|---|---|---|---|---|
| $N$ | $w_c$ | $w_s$ | $M_c$ | $M_s$ | $w_c$ | $w_s$ | $M_c$ | $M_s$ |
| 2 | 1.399 | 1.399 | 2.356 | 2.356 | 1.124 | 1.127 | 2.437 | 2.478 |
| 4 | 1.482 | 1.482 | 2.336 | 2.336 | 1.227 | 1.227 | 2.266 | 2.266 |
| 8 | 1.499 | 1.499 | 2.326 | 2.326 | 1.259 | 1.259 | 2.283 | 2.283 |
| 16 | 1.503 | 1.503 | 2.322 | 2.322 | 1.266 | 1.266 | 2.290 | 2.290 |
| Ref. | 1.505 | | 2.320 | | 1.26 | | 2.31 | |

## 8. Conclusions

The paper has discussed the computational efficiency of hybrid–Trefftz thick plate elements. An alternate domain-based formulation was introduced that allows elements to be formulated analytically. The use of energy-orthogonal internal approximations leads to a diagonal **H** matrix, and provides substantial computational efficiency. The domain-based formulation also leads to an alternate, simplified load vector that further improves the computational efficiency.

## Appendix

The non-zero terms of **G** are given below in Fortran format. Note that the following expressions are in the form generated by Reduce. Further computational efficiencies can be achieved by extracting common sub-expressions.

```
G(1,2)=D*(NU+1)*Y23
G(1,3)=D*(NU+1)*X32
G(1,5)=D*(NU+1)*Y31
G(1,6)=D*(NU+1)*X13
G(1,8)=D*(NU+1)*Y12
G(1,9)=D*(NU+1)*X21
G(2,2)=-D*(NU-1)*Y23
G(2,3)=D*(NU-1)*X32
G(2,5)=-D*(NU-1)*Y31
G(2,6)=D*(NU-1)*X13
G(2,8)=-D*(NU-1)*Y12
G(2,9)=D*(NU-1)*X21
G(3,2)=-D*(NU-1)*X32
G(3,3)=-D*(NU-1)*Y23
G(3,5)=-D*(NU-1)*X13
G(3,6)=-D*(NU-1)*Y31
G(3,8)=-D*(NU-1)*X21
G(3,9)=-D*(NU-1)*Y12
G(4,1)=-3*D*Y23
G(4,2)=((((Y12+Y23)*X13-(Y23+Y31)*X21)+4*A)*D)/2
G(4,3)=((Y12-Y31)*D*Y23)/2
G(4,4)=-3*D*Y31
G(4,5)=(-(((Y12+Y31)*X32-(Y23+Y31)*X21)-4*A)*D)/2
G(4,6)=(-(Y12-Y23)*D*Y31)/2
G(4,7)=-3*D*Y12
G(4,8)=(-(((Y12+Y23)*X13-(Y12+Y31)*X32)-4*A)*D)/2
G(4,9)=(-(Y23-Y31)*D*Y12)/2
G(5,1)=-3*D*X32
G(5,2)=((X13-X21)*D*X32)/2
G(5,3)=((((Y12-Y31)*X32+X13*Y12-X21*Y31)+4*A)*D)/2
G(5,4)=-3*D*X13
```

```
G(5,5)=((X21-X32)*D*X13)/2
G(5,6)=(-(((Y12-Y23)*X13-X21*Y23+X32*Y12)-4*A)*D)/2
G(5,7)=-3*D*X21
G(5,8)=(-(X13-X32)*D*X21)/2
G(5,9)=(-(((Y23-Y31)*X21+X13*Y23-X32*Y31)-4*A)*D)/2
G(6,1)=(D*(NU-1)*IX*X32)/(A*R+IX)
G(6,2)=(-(NU-1)*(X13-X21)*D*IX*X32)/(6*(A*R+IX))
G(6,3)=(-((X13*Y12-X21*Y31+X32*Y12-X32*Y31)+4*A)*D*(NU-1)*IX)/(6*(A*R+IX))
G(6,4)=(D*(NU-1)*IX*X13)/(A*R+IX)
G(6,5)=(-(NU-1)*(X21-X32)*D*IX*X13)/(6*(A*R+IX))
G(6,6)=(((X13*Y12-X13*Y23-X21*Y23+X32*Y12)-4*A)*D*(NU-1)*IX)/(6*(A*R+IX))
G(6,7)=(D*(NU-1)*IX*X21)/(A*R+IX)
G(6,8)=((NU-1)*(X13-X32)*D*IX*X21)/(6*(A*R+IX))
G(6,9)=(((X13*Y23+X21*Y23-X21*Y31-X32*Y31)-4*A)*D*(NU-1)*IX)/(6*(A*R+IX))
G(7,1)=(D*(NU-1)*IY*Y23)/(A*R+IY)
G(7,2)=(-((X13*Y12+X13*Y23-X21*Y23-X21*Y31)+4*A)*D*(NU-1)*IY)/(6*(A*R+IY))
G(7,3)=(-(NU-1)*(Y12-Y31)*D*IY*Y23)/(6*(A*R+IY))
G(7,4)=(D*(NU-1)*IY*Y31)/(A*R+IY)
G(7,5)=(-((X21*Y23+X21*Y31-X32*Y12-X32*Y31)+4*A)*D*(NU-1)*IY)/(6*(A*R+IY))
G(7,6)=((NU-1)*(Y12-Y23)*D*IY*Y31)/(6*(A*R+IY))
G(7,7)=(D*(NU-1)*IY*Y12)/(A*R+IY)
G(7,8)=(((X13*Y12+X13*Y23-X32*Y12-X32*Y31)-4*A)*D*(NU-1)*IY)/(6*(A*R+IY))
G(7,9)=((NU-1)*(Y23-Y31)*D*IY*Y12)/(6*(A*R+IY))
```

In the above expressions, $X_{ij} = x_i - x_j$ and $Y_{ij} = y_i - y_j$.

## References


[1] O.C. Zienkiewicz, R.L. Taylor. The Finite Element Method, volume 2. *Butterworth-Heinemann*, Oxford, fifth edition, 2000.

[2] S.P. Timoshenko, S. Woinowsky-Krieger. Theory of Plates and Shells. *McGraw-Hill*, New York, second edition, 1959.

[3] R.D. Mindlin. Influence of rotatory inertia and shear on flexural motion of isotropic plates. *Journal of Applied Mechanics*, **23**: 31–38, 1951.

[4] J. Petrolito. A modified ACM element for thick plate analysis. *Computers and Structures*, **32**: 1303–1310, 1989.

[5] J. Petrolito. Hybrid-Trefftz quadrilateral elements for thick plate analysis. *Computer Methods in Applied Mechanics and Engineering*, **78**: 331–351, 1990.

[6] J. Petrolito. Triangular thick plate elements based on a hybrid-Trefftz approach. *Computers and Structures*, **60**: 883–894, 1996.

[7] J. Jirousek, L. Guex. The hybrid-Trefftz finite element model and its application to plate bending. *International Journal for Numerical Methods in Engineering*, **23**: 651–693, 1986.

[8] J. Jirousek, A. Wroblewski, Q.H. Qin, X.Q. He. A family of quadrilateral hybrid-Trefftz p-elements for thick plate analysis. *Computer Methods in Applied Mechanics and Engineering*, **127**: 315–344, 1995.

[9] J. Jirousek. Improvement of computational efficiency of the 9 DOF triangular hybrid-Trefftz plate bending element. *International Journal for Numerical Methods in Engineering*, **23**: 2167–2168, 1986.

[10] T.J.R. Hughes, L.P. Franca. Convergence of transverse shear stresses in the finite element analysis of plates. *Communications in Applied Numerical Methods*, **4**: 185–187, 1988.